Colloid and Surface Science
2025, Vol. 7, No. 1, pp. 1-18
https://doi.org/10.11648/j.css.20250701.11

Research Article

Electrochemical and Nanoindentation Study of Manganese Oxide Nano-Particles Mediation on Corrosion Retardation of Citrus Extract on Carbon Steel in 15% HCl

Cyril Onyeka Okoye[1, *], Emmanuel Onche[2], Abdulhakeem Bello[3], Habitat Chaolu[4]

[1]African Development Bank Laboratory, African University of Science and Technology, Abuja FCT, Nigeria
[2]Department of Mechanical Engineering, University of Abuja, Abuja FCT, Nigeria
[3]Department of Theoretical and Pure Physics, African University of Science and Technology, Abuja FCT, Nigeria
[4]Department of Chemistry, Federal University of Agriculture, Makurdi, Nigeria

Abstract

Nanoparticles (NPs) are the center of attraction in all branches of science, engineering and technology. Therefore, in corrosion science, it is expected that (NPs) will solve the problem of replacement of chromates through inhibitor modification. Among the electrochemical techniques employed for analyses were electrochemical noise (EN), cyclic potentiodynamic polarization (CPP), electrochemical impedance spectroscopy (EIS), and linear polarization resistance (LPR). Other characterization methods such as structural phase analyses with x-ray diffractometer (XRD), functional group analysis with Fourier Transform Infrared (FTIR) spectroscopy and nanoindentation were employed. The synthesized material was identified as nanoparticles by structural phase and UV-vis absorption analyses. All the electrochemical techniques manifested escalation of inhibition efficiency (Z %) at the introduction of the (NPs). Almost all the evaluated synergism constants (S_Q) of each composite mixture of PECS and MnO_2NPs achieved values which are above the threshold of one used to indicate whether synergism or antagonism took place. Nano-indentation with a scanning probe microscope (SPM) shows that the carbon steel encountered highest protection from degradation in 15 % HCl containing both PECS and MnO_2NPs, followed by PECS and suffered the greatest degradation attack in the free acid medium. These results are full of prospects for a binary mixture of MnO_2NPs+PECS to be used as non chromate corrosion retardant and indicate that this inhibitor modification approach can serve as a substitute to the use of banned cancer-causing and environmentally damaging chemical inhibitors.

Keywords

Retardant, Corrosion Retardation, Carbon Steel, Polarisation, MnO_2NPs, PECS, Metal, Nano-Particles

[*]Corresponding author: cokoye@aust.edu.ng (Cyril Onyeka Okoye)

Received: 22 January 2025; **Accepted:** 8 February 2025; **Published:** 29 May 2025

1. Introduction

The trending options indicate that the present and next-generation research domains of metal corrosion technicians, engineers and scientists should be geared towards sustainability goals like circular materials economy, after all, economy is the main reason for any business [1]. A typical scenario is polishing the route to elongate the service duration of metals, non-metals and other construction materials by evolving modern engineering and scientific methods [1, 2]. Even though several researchers have advocated an integrated spectrum of experimentation, additive manufacturing and machine learning still yet applying the so called notion of 4-Rs, that is reuse-recycle-reduce-remanufacture meant to elongate the service life of metal through traditional experimentation is the best realistic approach [2]. Presently, Scientists from all 'works of knowledge' such as engineering, pharmacy, medicine, biotechnology, material science and so on, have focused their attention on nanotechnology and this has yielded diverse forms of metal based nanoparticles [3]. The most distinguishing feature of nanoparticles is their characteristic size range which is between 1 to 100 nanometers (nm). This size range is the reason adduced to their possession of special properties which are not found in ordinary macro materials [3-5]. At nano size range, materials are known to have improved surface to volume dimension, sophisticated mechanical properties, enhanced chemical activity, better optical properties and so on [4]. An important area of scientific research where nanoparticles have impacted and distinguished themselves from macro materials is in the field of corrosion retardation of substrate metal to mitigate deterioration in different belligerent service conditions [5]. Metal based nanoparticles have been synthesized from metallic based salts, oxides and bases and employed as synergistic agents to upgrade the inhibition efficacy of usual inhibitors such as polymers, surfactants, plant extracts and others [5-7]. The reason comes from the point of view of environmental friendliness, low cost, readily available, and a quest to occupy the performance gap created by Legislative bans on chromium vi and its associated derivatives [6]. These drove Quadri *et al* [7], to synthesize zinc nanoparticles from zinc oxide, composite it with different polymers such as polyacrylonitrile, poly-(vinylpyrrolidone) and poly(ethylene glycol), then they were tested as mild steel degradation inhibitor in an acidic electrolyte. For the 3 electrochemical techniques utilized, they obtained retardation efficiencies ranging from 64.08 to 90.81% of the optimum concentration, thus presenting zinc oxide nanoparticles as powerful synergistic agents. Solomon *et al* [8], participated in this green chemistry approach by compositing different concentrations of a mixture of silver nanoparticles and polymethacrylic acid and employed for aluminum degradation retardants in an H_2SO_4 environment. At optimum concentration for gravimetric and electrochemical techniques, the retardation efficiencies obtained range from 60 to 85.6 %. Obot *et al* [9], synthesized honey/silver nanoparticles (AgNPs) under the valuable interference of sunlight and investigated its synergism for improved retardation of metallic material degradation in a belligerent environment. With polarisation characterization technique the Z % improved significantly from 78.4 of 2 % v/v to 91.6 % of optimum concentration. Azzam *et al* [10], chemically derived a polymer based surfactant, called poly 12-(3-amino phenoxy) dodecane-1-thiol which arranged voluntarily on a medium containing AgNPs. When scrutinized as non-harmful carbon steel metal degradation retardants in an acidic environment utilizing gravimetric and electrochemical experiments, the outcome indicates that (Z %) exhibited by the composite binary mixture of the polymer based surfactant and AgNPs is higher than those from the surfactant alone, thus inferring that synergism took place.

Numerous corrosion inhibition research dealing with synthesis and use of nanoparticles for corrosion retardation have preferentially chosen AgNPs without stating its special quality over others, even though other nanoparticles may possess properties and easier synthesis route better and over those of AgNPs. Manganese oxide nanoparticles (MnO_2NPs) are oval-shaped high surface area metal nanoparticles, with diameter between 20-40 nm and total surface area in the range of 30 to 50 m^2/g [11]. Manganese materials had been used by corrosion scientists for corrosion inhibition of different metals, for example Jian *et al* [12], investigated to unravel corrosion retardation behavior possessed by 3 manganese based retardants namely, Manganese - cerium - polyphosphate, manganese - polyphosphate and manganese - cerium conversion coatings on LZ91 magnesium alloy. In their findings Mn-Ce-P formulation reduced the metal degradation surface to approximately 10 % with a 72 hr period of salt spray test conducted on LZ91 Mg based alloy. This clearly demonstrated that manganese materials are a potential source of nano-material for anti-corrosion application in industries. Therefore, as corrosion scientists battle to discover corrosion inhibitors that will challenge the performance height achieved by banned chromium vi and other harmful corrosion retardants, consideration of manganese nano-material mediation on plant extracts is another alternative. Kadar *et al* [13], employed ultra-sonication method to obtain some alkaloids from withered rose and lotus flowers and used them to synthesize MnO_2NPs from manganese acetate. When formed into paste and tested as metal degradation retardant in an acidic solution, with polarization technique they yielded (Z %) of 72.63 % and 51.50 % from the free acid solutions.

Plant extracts are considered the best group of green corrosion retardants because they are easily available, cheap and environmentally friendly. Not only these, they are non-harmful, non-toxic compounds, they are decomposable, they are replenishable source of materials and they contain phytochemicals such as alkaloids, amino acids, tannin and pigments which exhibit inhibitory functions [14]. Almost all

these phytochemicals are needful in corrosion chemistry based on their heterocyclic organic contents with electronegative functional groups most of which possess π-electron bond system and heteroatoms such as oxygen, sulfur, nitrogen including aromatic moieties in their matrices [15]. These chemical structures make plant extracts endearing materials for corrosion inhibition of metals. There were several scientific reports on the improvement of (Z %) of plant extracts by metal based nanoparticles. Hence it is suggested that the improvement of the inhibition potent in (Z %) of plant extracts brought about by introduction of MnO_2NPs was caused by influence of the nanoparticles to stabilize the accumulated extract film on substrate cross sections [3].

2. Research Materials and Methodology Used

2.1. Preparation of Carbon Steel

All the experiments were conducted with the steel coupons cut into rectangular shape of dimensions 35.8 x 29.5 x 2.6 mm and surfaced by polishing with sandpapers of grades 600, 800, and 1200. Thereafter, they were washed under running water with detergent, scrubbed with acetone, and stored in a dust and humidity-free desiccator ready for duty. The composition in percentage by weight of the substrate metal engaged for these tests are as follows: C (0.195), P (0.018), Mn (0.023), S (0.019), Si (0.062), Cu (0.126), Zr (0.013) and the balance is Fe (99.544).

2.2. Synthesis of Corrosion Inhibitor

Orange peels were collected from a fruit dealer at Garki Model Market, Abuja FCT, Nigeria, washed with detergent, and rinsed severally with plenty of distilled water, before being left to sun-dry. After crushing and sieving in Retch machines, 5 g of the fraction that passed through a 45 µm sieve was taken and dissolved in 200 ml of 0.5 M methanol, then refluxed at 60 ℃ for 24 hours. The deposit obtained was separated from methanol by centrifuging at 2000 rpm for 7 minutes, decanted, washed, and dried at 60 ℃ to obtain an ash-colored solid. To ensure solubility in an acid electrolyte, the extract was further crushed with agate mortar and pestle. The concentrations prepared were 200, 400, 600, 800 and 1000 ppm in 15 % HCl.

2.3. Synthesis of MnO_2 Nanoparticles

10 mg of activated carbon (Kuraya, Madrid, Spain) was dissolved in 100 mL of 0.05 M potassium permanganate ($KMnO_4$) powder (BDH, Poole, England), using a round-bottom flask, arranged on a hot plate with magnetic stirring rod and connected to a refluxing unit at 160 ℃ for 2 days with continuous magnetic stirring. 0.2 M KCl solution was added during the washing process to remove the potassium component of the permanganate solution, and later dried in an oven at 80 ℃. Different concentrations of the *citrus sinensis* extract from 200 to 1000 ppm were prepared with 15% HCl solution before the introductions of 2.5 mm MnO_2NPs to form the binary synergized counterpart.

2.4. Functional Group Analysis

FTIR spectra of all samples in this study were recorded employing a Thermo-Scientific equipment, 600 model Nicolet with i-D 1 device for solid transparent specimens which was controlled using the OMNIC 9 spectroscopy software (Thermo Scientific, Verona, Madison, USA). Measurements were performed at a sweep rate of 4 cm^{-1} and a transmittance region of 500 to 4000 cm^{-1} wavenumber. Before this analysis, pellets were prepared by grinding the rusts peeled from the coupons from blank and maximum concentration solutions with KBr in an agate mortar with pestle for concentration dilution measure and to achieve high quality spectra.

2.5. Absorption Studies

Absorption studies were carried out employing an Ultra violet visible (UV - vis) spectrometer: Specord 300 series (Analytik, Endress-Hauser, Jena, Germany) with 2 chambers, one for the reference (deionized water) and the other for the measured solution. The dilute solution being measured was prepared by dissolving a few particles of MnO_2NPs in deionized water. After initialization and calibration, scanning was done from a wavelength of 200 to 700 nm and a sweep rate of 4 cm^{-1}.

2.6. Electrochemical Techniques

A glass-made electrochemical cell container was employed to house the electrolyte and the 3 electrodes arrangement. This is made up of a silver/silver chloride reference electrode containing 3.5 M KCl solution, a 50 mm long by 8 mm diameter graphite rod functioned as a counter electrode and the carbon steel denoted as the working electrode with an experimented area of 20 mm^2. All electrochemical measurements were performed on at least 3 samples per solution on the multichannel potentiostat, VMP Biologic SP-300 model (BioLogic, Seyssinet, Paris, France), controlled with EC Lab software at room temperature of 2 ℃.

2.6.1. Cyclic Potentiodynamic Polarisation (CPP)

CPP curves were acquired for each electrolyte solution after 1 hr for stabilization of the open circuit voltage (E_{OCV}) by performing the reduction / cathodic (green colour) and the oxidation / anodic (yellow colour) polarization scans. Prior to this step an excitation voltage of 10 mV was passed through the cell, then the reduction process was measured commencing from +50 mV to −500 mV with respect to the E_{OCV} while the oxidation process was also scanned from −50

mV to +500 mV also with respect to the E_{OCV} and maintaining an inter-exchange point proximate to the E_{OCV}. The scan rate applied was 0.1667 mV/s with a measurement gathering data point of 5 per s. The Tafel fitting procedures were performed from the analysis button of the EC Lab software to evaluate corrosion variables such as the corrosion voltage (E_{corr}), the current density (i_{corr}) and other Tafel variables including reduction Tafel constant (β_c), oxidation Tafel constant (β_a) and the degradation rate (C_R).

2.6.2. Electrochemical Impedance Spectroscopy (EIS)

EIS experiments were carried out on all sample solutions after stability of the electrochemical system for an OCV period of 10 mins from a frequency region of one hundred kHz to ten mHz with an initial sinus of 10 mV with respect to E_{OCV}. Measurements were performed for 42 data points. Analysis of data was done using the Z_{fit} incorporated in the analysis button of the EC Lab software. The impedance data were fitted with different equivalent circuit diagrams and equations, after 5000 iterations the software issued out the electrochemical parameters whose fitting is determined by the value of CHI square obtained.

2.6.3. Linear Polarization Resistance (LPR) Imposed on Open Circuit Voltage (OCV)

The OCV was monitored for 1 hr, while performing an imposed LPR measurement with an excitation signal of 10 mV with respect to the OCV at a sweep rate of 0.1667 mV/s on the free acid and inhibited solutions. The polarization resistances (R_p) were evaluated from the slope of the voltage against current graph at the corrosion potential (E_{corr}) by performing R_p fit from the analysis button of the EC Lab software.

2.6.4. Electrochemical Noise (EN)

A three electrode arrangement was used for the EN experiments with two coupons of carbon steel, where one served as working electrode and the other as counter electrode with an Ag/AgCl containing 3.5 M KCl which functioned as a reference electrode. Electrochemical measurements were done after an OCV period of 1 hr for equilibrium to be established between the 3 electrodes. The total points of data gathered for a sweep rate of 1 data per second was 1024. The lowest and highest regions of the zero resistance ammeter (ZRA) were manually evaluated throughout the experiment with a lowest region of 1 nA and the highest region of 100 µA.

2.7. Nanoindentation Analysis

A Triboindenter, model Ti950 (Brucker, Germany) operating in load function state with a Berkovich indentation probe was employed to assess the tribology/contact mechanics properties of the metal samples. Prior to this, the carbon steel coupons were prepared for nanoindentation analyses by immersing in the blank and optimum concentrations for 24 hrs, before rinsing with distilled water and drying in an oven. Several positions were measured on a sample specimen by the triboindenter with 10 mN value of peak load and 250 µN/s as value of rate of unloading/loading. The indenter was positioned at this force for 50 s. A distance of 10 µm separated each of the indent positions while the scanning probe microscope (SPM) at the same time was used to obtain the corresponding microstructural images of the samples.

2.8. Analysis of Structural Phase

The X-ray grazing phenomena was performed with the radiation, Cu-Kα for the purpose of analysing the structural variations of the MnO_2NPs employing a Malvern designed Panalytical's instrument X'Pert³ MRD model (Malvern, Holland) operating at wavelength of 1.62 A and voltage of 50 kV. The equation ascribed to Debye-Scherrer was employed to evaluate the crystallite size diameters.

3. Results and Discussions

3.1. Analysis of Chemical Properties of MnO_2NPs and Corrosion Products

Figure 1 (a) shows the structural phase spectrum of the synthesized MnO_2NPs. The spectrum manifests the presence of pyrolusite, also known as β phase MnO_2, a polymorphic MnO_2. The diffraction bands are aligned with the XRD identities of JCPDS Card identity which is 00-002-0567. Debye-Scherrer's method [13], was used to calculate the particle diameters given as (3.128 Å), an evidence that the synthesized MnO_2 is a nanoparticle. Signal processing for peak fitting and correction of the base line was done on OriginLab graphic software.

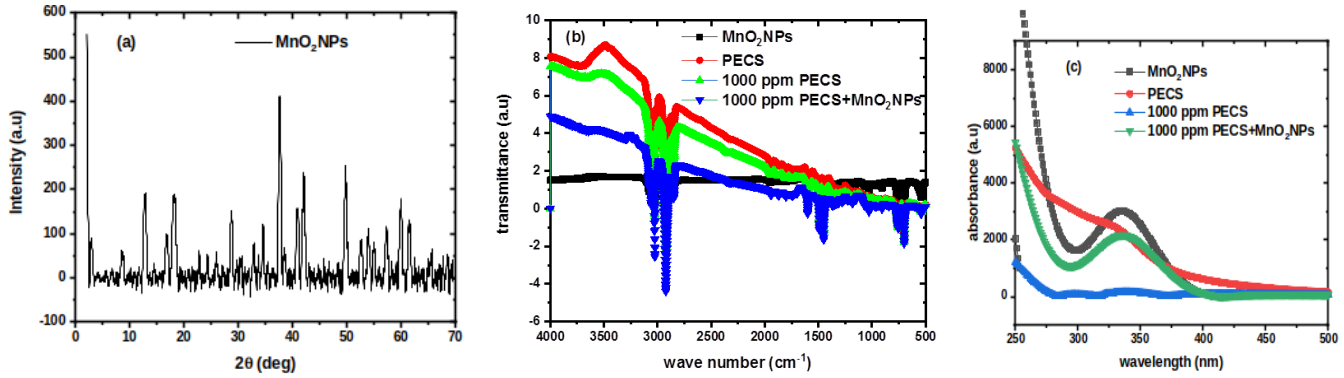

Figure 1. *(a) XRD spectrum of the MnO_2NPs, (b) functional group spectra and (c) absorption spectra of the MnO_2NPs, PECS and corrosion products.*

Figure 1 (b) exhibits the FTIR spectra of MnO_2NPs, PECS and the rusts from carbon steel soaked in the optimum concentrations for 24 hrs. The possession of numerous bands by PECS and its associates confirms the ligno-cellulose nature of the biomass extract. The peak like a 'trough' between 3850 and 3400 cm^{-1} is in the region of either hydroxyl or amine functional groups. Nevertheless, with the existence of a narrow intensity at almost 3600 cm^{-1}, it can be ascribed to an oxygen-containing group such as hydroxyl [8]. The existence of the methylene/methyl group is manifested by the bands with centers at 3080 and 2850 cm^{-1}, suggesting levels of ring saturation. The low intensity band at 535 cm^{1} in the spectrum of the nanoparticles is an indication of the existence of inorganic metal containing group [7].

The UV vis absorption spectra of MnO_2NPs and the optimum concentrations of PECS and MnO_2NPs+PECS batches are shown as Figure 1 (c). The broad band between 324 and 385 cm^{-1} indicates an absorption characteristic of a nanoparticle [7, 8]. Obot *et al*, [9], have suggested that the syndrome of surface plasmon resonance (SPR) exhibited by nanoparticles at many absorption regions in the ultraviolet visible spectrum is a manifestation of their orderly mode of light absorption and the behavior of electromagnetic field formed as a result of uniform vibration of charged electrons.

3.2. Open Circuit Voltage (OCV)

The working electrode was permitted to achieve equilibrium with the reference electrode for 30 mins before a perturbation voltage of 10 mV was passed through the circuit. The voltage vs time plots of the various concentrations with error bars were shown in Figure. 2. The plots exhibited horizontal linear lines throughout the duration, suggesting no change in mechanism. The voltage shift relative to that of the blank is a recognized tool in corrosion science to characterize the behavior of a particular corrosion system as either anodic, cathodic or mixed inhibition [10]. The voltage shifts of the samples with reference to that of the blank for system (a) range from −0.01 to -0.59 mV while for system (b) it is from −0.01 to -0.29 mV. The voltage shifts are all less than -85 mV, which confirms that PECS and its mixture with MnO_2NPs inhibits both anodic and cathodic reactions, that is mixed inhibition.

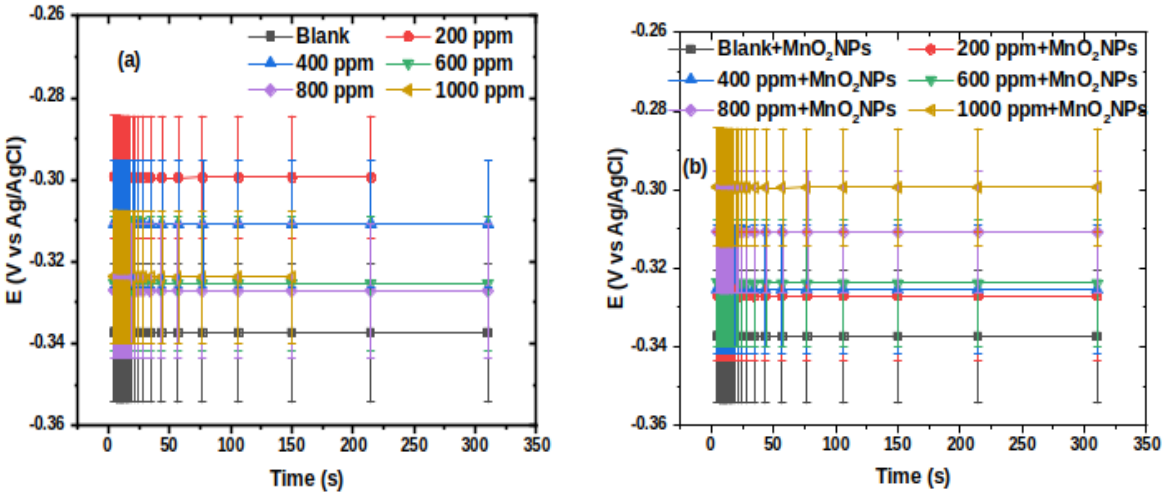

Figure 2. *OCV variations with time at 5 % error bars for the systems (a) PECS and (b) PECS+MnO_2NPs.*

3.3. Cyclic Potentiodynamic Polarization (CPP) and Linear Polarization Resistance (LPR)

Figure 3 (a) and (b) present the CPP curves with error bars of the electrochemical system for the degradation retardation of carbon steel in an aggressive medium of 15 % HCl by (a) PECS and (b) PECS+MnO_2NPs. The Tafel corrosion parameters were obtained by performing linear extrapolation of the reduction and oxidation branches of the potentiodynamic curves. The slopes of the two (2) tangential lines gave the oxidation (β_a) and reduction (β_c) Tafel constants. The reduction/cathodic arm represents an evolution of the hydrogen gas process and the second arm the oxidation/anodic branch represents the dissolution of the carbon steel [7]. The two curves meet and form a horizontal line which indicates an inter-exchange point between oxidation and reduction processes or the other way round for a second potentiodynamic cycle. To examine the quality of PECS alone and its mixtures with MnO_2NPs for degradation retardation of carbon steel in 15 % HCl the electrochemical parameter, current density (i_{corr}) was employed. The value of i_{corr} is dependent on some characteristics of the corrosion retardation systems such as chemical and physical compositions of working electrode, electrolyte composition, process variables like pressure, temperature and so on [10, 15]. The retardation efficiency (Z %) is given by equation (1) [6-9]:

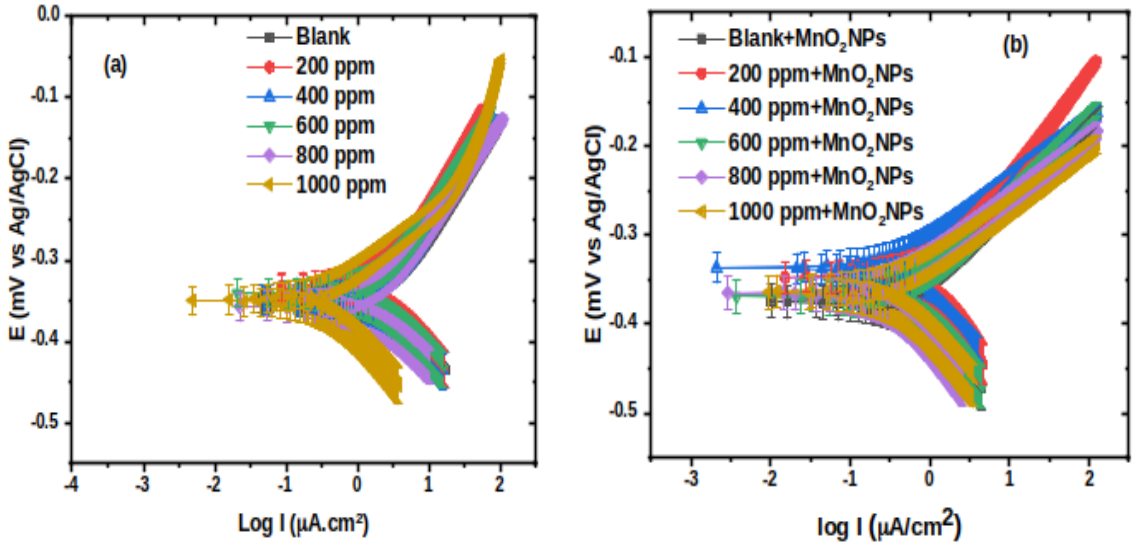

Figure 3. *CPP plots of the carbon steel corroding in free acid, inhibited and synergized solutions.*

$$Z_{\%} = \left(\frac{i^{b}_{corr} - i^{a}_{corr}}{i^{b}_{corr}}\right) x100 \qquad (1)$$

Where i^{b}_{corr} represents the current density of the free acid electrolyte and i^{a}_{corr} represent current densities of inhibited added electrolytes.

The calculated (Z %) and the values of other electrochemical variables were exhibited in Table 1. The values of i_{corr} are inversely proportional to both the retardants' concentrations and the corrosion retardation efficiencies, this is an indication that corrosion retardation took place through adsorption process which lead to formation of film covering the metal cross-sections [9]. The (Z %) of PECS+MnO_2NPs are higher than PECS alone, suggesting that the NPs containing composite adsorbs better and easier on the cross-sections of the carbon steel than PECS alone, leading to elevated (Z %). This also confirms strong interaction by bonding between the NPs and the electronic lattices of the steel resulting in improved adsorption and higher surface coverage [6, 7]. The overlapping of the potentiodynamic curves in Figure 2 and their close resemblance indicate no change in reaction mechanism throughout the inhibition processes. Even though no general pattern can be drawn in the variations of E_{corr} of additive solutions with respect to E_{corr} of free acid solution, the highest value of this shift for system (a) is -27.78 mV while for system (b) it is -16.01 mV. These values are less than -84 mV which is the threshold used by corrosion scientists to determine whether an inhibitor is either mixed, anodic or cathodic form [14]. This suggests that PECS and PECS+MnO_2NPs inhibit both oxidative carbon steel dissolution and reductive evolution of H_2 gas processes and are therefore mixed types of inhibitors. However, the anodic arm is longer and more prominent, moreover the values of β_a are higher than β_c at all concentrations thereby indicating oxidation process domination.

According to Stern-Geary equation [16] the current density is related to both polarization resistance and Tafel constants in the following manner;

$$R_P = \frac{\beta_a \beta_c}{i_{corr} x 2.3(\beta_a + \beta_c)} \quad (2)$$

Here R_p represents the resistance to polarization, i_{corr} represents the current density whereas β_c and β_a represent the oxidation and reduction Tafel constants respectively. This equation reflects the relationship between the two polarization techniques in Table 1, in which i_{corr} is inversely related to R_p and decreases with increments in concentration while R_p increases with corresponding increments in concentration. The introduction of the NPs into the different concentration diminished the i_{corr} down to its lowest value of 602.24 µA cm^2 at optimum concentration and elevated the R_p value to 66.50 Ω cm^2 which are 60.75 % reduction and 58.56 % elevations respectively above the optimum concentration of PECS only which are 991.29 µA cm^2 and 38.94 Ω cm^2 respectively. The non-alignment extent of reduction and increment of i_{corr} and R_p between PECS and MnO_2NPs+PECS can be attributed to variations in electrochemical parameters that will be fully dealt with in the comparison of electrochemical techniques below. The rate of corrosion was calculated from equation (3) [16] as,

$$C_{R(mmpy)} = \frac{0.00327 x i_{corr}(E_q)}{\rho_m . A} \quad (3)$$

Here E_q is the carbon steel's equivalent weight, 27.85 (g/mm), i_{corr} is the current density in (µA.cm^2), ρ_m is the carbon steel's density given as 7.85 (g/cm^3), A is carbon steel coupon's total surface area, 20 (mm^2) and 0.00327 is a corrosion constant related to C_R.

Table 1. *CPP and LPR electrochemical techniques' variables of carbon steel corroding in control, inhibited and synergized solutions.*

System of inhibitor	CPP					LPR		
	E_{corr} (mV vs Ag/AgCl)	I_{corr} (µA. cm^2)	βa (mV/dec)	βc (mV/dec)	Z (%)	C_R (mmpy)	R_P (Ω cm^2)	Z (%)
PECS control	-347.64	2 795.89	138.4	108.7		1.62	13.8	
200 ppm	-333.18	1 574.53	122.1	91.2	43.68	0.91	16.53	16.52
400 ppm	-349.06	1 416.71	131.9	98.8	49.32	0.82	19.82	33.72
600 ppm	-340.52	1 300.39	152.8	114.3	53.48	0.75	27.94	50.61
800 ppm	-356.77	1 121.06	165.9	126.6	59.90	0.65	35.21	60.81
1000 ppm	-375.42	991.29	149.9	112.6	64.54	0.58	38.94	64.56
control+MnO_2NPs	-374.08	1 296.55	90.4	112.6	53.62	0.75	24.14	42.83
200+MnO_2NPs	347.12	904.31	71.0	117.6	67.65	0.53	28.96	52.34
400+MnO_2NPs	-336.54	891.27	71.1	103.2	68.12	0.52	34.71	60.24
600+MnO_2NPs	-368.93	780.44	66.1	109.5	72.08	0.45	47.62	71.02
800+MnO2NPs	-364.91	642.51	93.2	125.7	77.02	0.37	59.38	76.50
1000+MnO_2NPs	-363.65	602.24	124.7	180.4	78.45	0.35	66.50	79.24

The LPR curves of the 2 systems of inhibitors are exhibited in Figure 4 (a) and (b) together with the possible observable error bars. A numerical fit of the curves yield the polarization resistance, R_p which were shown in Table 1. R_p increases with the chemical retardants' concentrations. That is, as more molecules of the plant extract and nanoparticles accumulate by adsorption on the cross-sections of the substrate to form a material barrier, the resistance to hydrogen gas emissions, oxidation and other side reactions that promote metal exfoliation increases [7]. Evaluation of the progress of polarization was made with retardation efficiency given by equation (4) [9]:

$$Z_{\%} = \left(\frac{R_p^a - R_p^b}{R_p^a}\right) x100 \quad (4)$$

Here R_p^a represents the resistance to polarization of the inhibitor added solution and R_p^b stands for the resistance to polarization of the free acid solution.

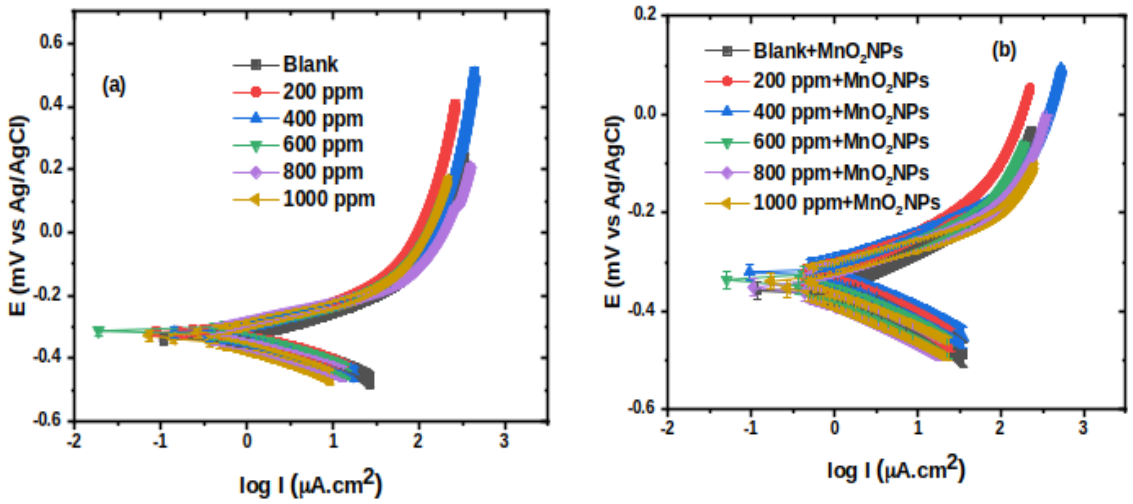

Figure 4. *LPR plots of carbon steel corroding in free acid, inhibited and synergized solutions.*

3.4. Electrochemical Impedance Spectroscopy (EIS)

The Nyquist impedance, Bode modulus and phase angle plots for the 2 sets of inhibitor systems were shown as Figures 5, 6 and 7 respectively, together with their associated error bars. For these 3 sets of figures and regarding Table 2, the Nyquist plots pseudo-semicircles, the S-shaped loops of Bode impedance plots and the bell shaped loops of phase angle plots all increase in size as the inhibitor concentrations and retardation efficiencies increase and as synergism takes place. For example, the Nyquist plots of PECS system increased from 4.63 Ω.cm^2 of the free acid solution to 18.38 Ω.cm^2 at optimum concentration of PECS while PECS+MnO_2NPs escalated to 37.02 Ω.cm^2 also at optimum concentration. These suggest mass and charge transfer activities leading to continuous formation of more layered coatings on the substrate cross-sections with the improvement of additives concentrations resulting in enhancement of corrosion retardation [14, 15]. The accumulation of inhibitor ions and molecules by the process of adsorption enhanced significant increments in resistance to polarization and noticeable reduction in the rate of the steel degradation [15]. Different forms of equivalent electric circuits arrangements composed of passive elements such as electrolyte resistance, R_{sol}, constant phase element Q_{cp}, and resistance to charge transfer, R_{ctrt} in series or parallel configurations were examined. The obtained data fitted more perfectly with Figure. 8, represented with the expression R_{sol}+$Q_{cp,}$/R_{ctrt}. This means the solution resistance is arranged to a parallel connection of the charge transfer resistance with the constant phase element. The double layer capacitance (C_{dl}) was replaced with a constant phase element (Q_{ctr}) to take care of macroscopic presence of impurities and imperfections on the working electrode cross-sections caused by corrosion attacks and other side reactions [14-17]. From Nyquist and Bode plots, at both high and low frequencies, the equivalent circuit manifested resistive and inductive characteristics respectively. The intersection of the high frequency line of Nyquist spectra with the real x-axis, yields electrolyte resistance (R_{sol}) while the intersection of the inductive line with the same real axis gives rise to charge transfer resistance (R_{ct}) [18]. As illustrated by Nyquist spectra and Bode modulus plots the high frequency and the low frequency regions meet at a point of intersection known as (f_{max}), whose values decrease down Table 2, as the inhibitor concentration and efficiencies increase. An assessment of the corrosion retardation of the carbon steel was made by using R_{ct} to calculate the retardation efficiencies utilizing equation (5) [17]:

$$Z_{\%} = \left(\frac{R_{ct}^{a} - R_{ct}^{b}}{R_{ct}^{a}}\right) x100 \quad (5)$$

Here R_{ct}^{b} and R_{ct}^{a} are the resistances to charge transfer of the free acid and the inhibited or synergized solutions respectively.

For comparison with polarization techniques, R_p values were evaluated by manipulating the difference between the impedance performed at the optimum and the impedance at minimum frequencies according to: equation (6) [19].

$$R_p = Z'_{(o)} - Z''_{(\infty)} \quad (6)$$

Here $Z'_{(o)}$ is the impedance at 100 kHz and $Z''_{(\infty)}$) is the impedance at 10 mHz. R_p was promoted with increase in concentration and the introduction of the nanoparticles. The C_{dl} is related to the variable of constant phase element by equation (7) [6-10]:

$$C_{dl} = Y_o(j\omega)^{-n} \quad (7)$$

Here Y_0 is taken as a CPE variable, α is the CPE power exponent, often used to gauge the extent of roughness or imperfections of the metal cross-sections, j^2 is equal to unity is

an imaginary number and ω is radian frequency of angle in rad^{-1}. The values of α_2 established a direct relationship with both concentration and (Z %) suggesting that as more layers of PECS and MnO_2NPs are occluded on the cross-sections of the carbon steel, roughness was diminished because contact points for corrosion manifestation are reduced [8-10].

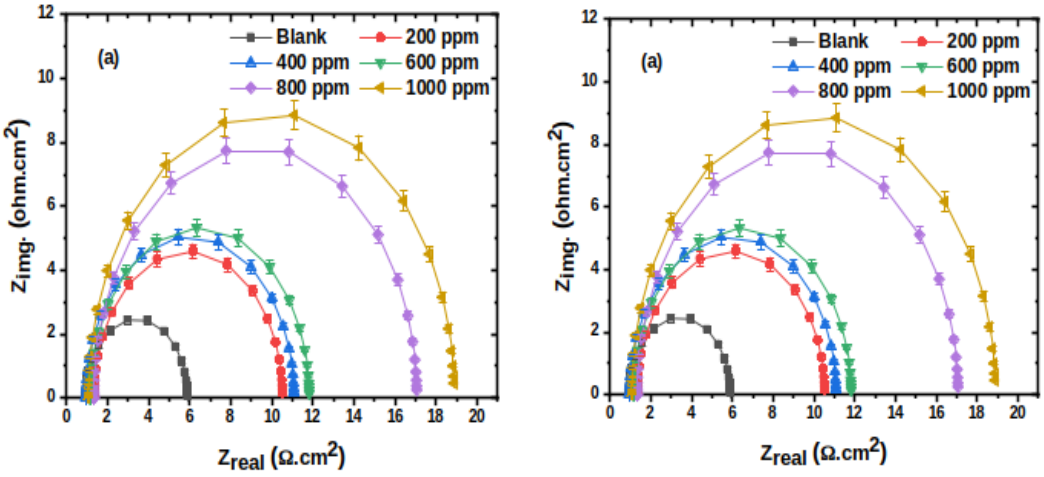

Figure 5. *Nyquist spectra with 5 % error bars of the carbon steel corroding in control, inhibited and synergized electrolytes.*

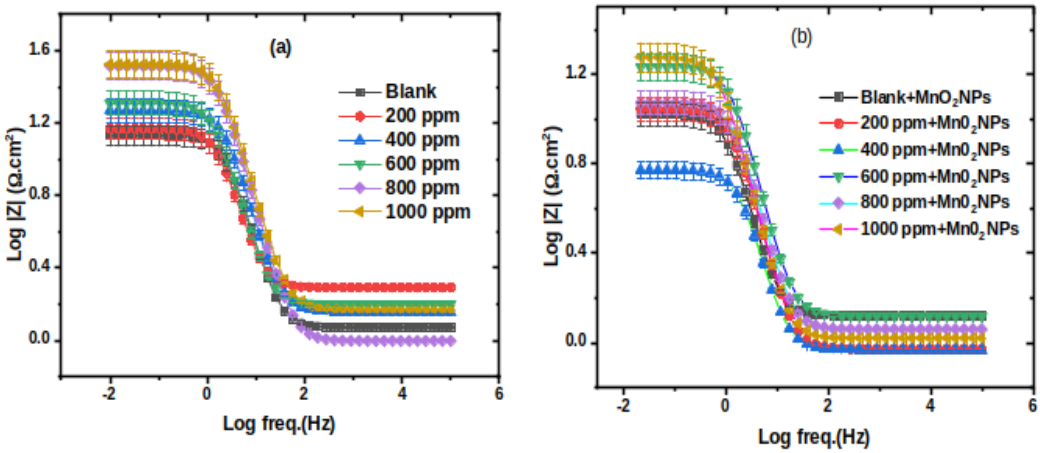

Figure 6. *Bode impedance plots with 5 % error bars of carbon steel corroding in control, inhibited and synergized electrolytes.*

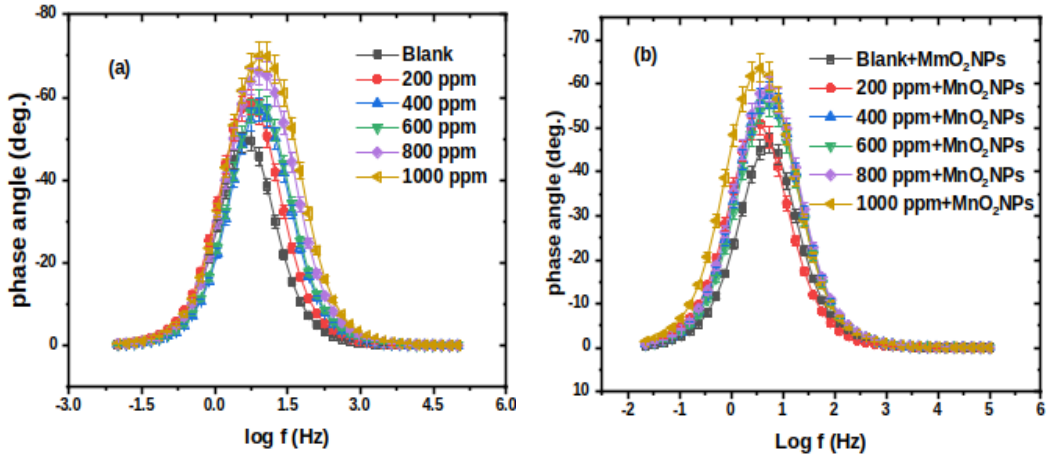

Figure 7. *Phase angle graphs with 5 % error bars of carbon steel corroding in control, inhibited and synergized solutions.*

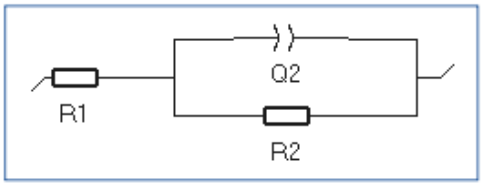

Figure 8. *Equivalent electric circuit of corrosion inhibition of the carbon steel.*

Bode plots of the substrate in the free acid and inhibited solutions exhibited almost the same pattern of behavior, they manifested significant reduction in the values of their impedance at the optimum frequency range between 100,000 to 100 Hz and a steady reduction in the median frequency region between 100 to 1 Hz. The phase angle plots exhibited a one-time constant only at the middle point between the optimum and low frequency range of the spectra. This single dominating time-constant is representative of corrosion phenomena such as the impact of adsorption on the boundary layer and the migration of the inhibitor ions and molecules into the solution [16, 18, 19]. The decrease in impedance modulus in terminal frequency ranges can be related to the reduction and phase angle shifts done by the time constant toward lower frequencies. Therefore, the reduction in metal degradation experienced by the carbon steel due to introduction of PECS and MnO_2NPs into the reference electrolyte can be ascribed to these phase shifts.

Table 2. *EIS variables for carbon steel corroding in control, inhibited and synergized solutions.*

System of inhibitor	R_{Sol} ($\Omega.cm^2$)	R_{ct} ($\Omega.cm^2$)	R_p ($\Omega.cm^2$)	Q_2 10^{-3} [$F.s^{(a-1)}$]	f_{max} (Hz)	α_2	CH^2	Z (%)
PECS control (0)	0.95 ±0.23	4.63 ±0.52	3.67	0.047 ±0.04	1.66	0.88 ±0.96	0.06	
200 ppm	0.92 ±0.24	5.44 ±0.54	4.52	0.025 ±0.02	1.66	0.89 ±0.91	0.09	18.75
400 ppm	0.95 ±0.02	10.92 ±0.52	9.97	0.015 ±5.67	1.12	0.89 ±0.84	0.33	63.14
600 ppm	1.20 ±0.23	11.66 ±0.53	10.46	0.014 ±4.97	1.12	0.90 ±0.79	0.01	64.87
800 ppm	1.41 ±0.23	16.33 ±0.50	14.92	0.012 ±2.28	1.12	0.92 ±0.96	0.65	75.38
1000 ppm	1.17 ± 0.22	18.38 ±0.47	17.21	0.011 ±2.31	0.76	0.93 ±0.99	0.63	78.65
PECS+MnO_2NPs Control (0)+ MnO_2NPs	1.31 ±0.22	9.51 ±0.51	8.19	0.02 ±7.32	1.11	0.89 ±0.98	0.35	55.17
200 ppm + MnO_2NPs	1.90 ±0.23	14.44 ±0.55	12.54	0.01 ±3.26	1.12	0.81 ±0.65	0.47	70.69
400 ppm + MnO_2NPs	1.36 ±0.24	18.99 ±0.53	17.63	7.21 ±1.52	1.66	0.83 ±0.63	0.29	79.16
600 ppm + MnO_2NPs	1.51 ±0.23	21.31 ±0.54	19.79	9.86 ±1.61	1.12	0.83 ±0.62	0.81	81.44
800 ppm + MnO_2NPs	0.90 ±0.24	36.25 ±0.54	35.35	5.40 ± 0.53	1.12	0.82 ±0.56	0.65	89.61
1000 ppm + MnO_2NPs	1.38 ±0.24	37.02 ±0.55	35.64	5.31 ±0.51	1.12	0.79 ±0.55	0.79	89.69

3.5. Electrochemical Noise (EN)

The EN analysis was conducted at time domain to investigate the metal degradation retardation phenomena, and use time variations of other variables to bring out information about the parameters of degradation. Figures. 9 (a) and (b) depict voltage (E) vs time (t) graphs of the steel substrate degrading in 15 % HCl medium and with the introduction of inhibitive and synergistic agents. In all the experiments, the voltage drops as time elongates. The electrochemical noise parameters were obtained by performing EN analyses from the analyses button of EC Lab software and were presented in Table 3. The magnitude of potential noise indicates the level of corrosion attack on the steel cross-sections [20]. The concentration of the inhibiting additives and the retardation efficiencies established an inverse proportional relationship with the electrochemical noise resistance (R_n). This suggests that the introduction of adsorbing chemical corrosion retardants ameliorated the electrochemical noise which is electrochemically related to the polarization and charge transfer resistances [21].

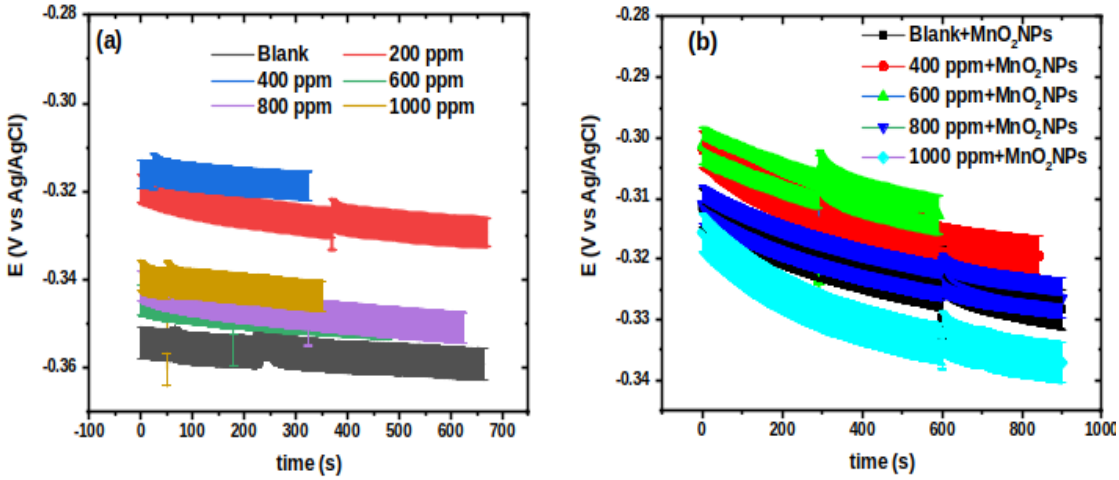

Figure 9. *EN plots with 5 % error bars of carbon steel corroding in control, inhibited and synergized solutions.*

Several published corrosion research works have stated that R_n values are inversely proportional to the values of polarization resistance R_p [16]. Hence the reciprocal of R_p in unit of ohm (Ω) is equal to R_n, these are directly proportional to the metal's rate of corrosion, when applied to equation of Stern-Geary [16, 20]. Hence, an improvement in the values of $1/R_n$ indicates low electrochemical phenomena on the cross sections of the carbon steel [20].

Table 3. *EN variables for carbon steel corroding in control, inhibited and synergized solutions of PECS and MnO_2NPs.*

System of inhibitor	Rn (Ω)	σ, (E_{we}) (V)	σ. (I) (A)	σ, (I)/rms(I)	R_p (10^{-3} x Ω.cm^2)	Z (%)
PECS system control (0)	312.9	$3.093x10^{-6}$	$10.12x10^{-9}$		3.19	
200 ppm	237.88	$6.08x10^{-6}$	$19.43x10^{-9}$	58.81	4.20	23.97
400 ppm	174.84	$22.17x10^{-6}$	$14.94x10^{-9}$	76.5	5.71	44.12
600 ppm	140.88	$12.26x10^{-6}$	$0.32x10^{-6}$	3.53	7.09	54.97
800 ppm	115.2	$32.99x10^{-6}$	$31.36x10^{-9}$	35.8	8.68	63.18
1000 ppm	108.2	$1.86x10^{-6}$	$0.20x10^{-6}$	5.482	6.74	65.42
PECS+MnO2NPs control+MnO2NPs	148.21	$7.81x10^{-6}$	$0.11x10^{-6}$	0.769	6.74	52.63
200 ppm+MnO2NPs	119.05	$20.45x10^{-6}$	$18.51x10^{-9}$	59.37	8.39	61.95
400 ppm+MnO2NPs	102.49	$2.122x10^{-6}$	$18.87x10^{-9}$	58.98	9.75	67.24
600 ppm+MnO2NPs	91.91	$6.823x10^{-6}$	$15.18x10^{-9}$	75.3	10.96	70.62
800 ppm+MnO2NPs	84.67	$3.093x10^{-6}$	$11.13x10^{-9}$	2.01	11.81	72.94
1000 ppm+MnO2NPs	81.05	$9.093x10^{-6}$	$12.19x10^{-9}$	5.31	12.33	74.09

The inhibition efficiency was evaluated with equation (8) given by:

$$Z_{\%} = \left(\frac{R_n^b - R_n^a}{R_n^b}\right) x100 \quad (8)$$

Here R_n^b and R_n^a are the noise resistances of the substrate in the free acid and inhibitor-added electrolytes respectively.

3.6. Comparison of Electrochemical Results with (Z %) and (R_p)

There had been several debates in electrochemistry about

how dependable the experimental data obtained in each electrochemical technique. In this work we used error bars and CH^2 to assess the quality of the parameters obtained in EIS technique, while in the other techniques we used both error bars and range of ± sign to indicate the level of validation of the experimental data. Secondly, by the study of experimented parameters common to the various techniques, good judgments can be made about the effectiveness of one technique over another. In this work the maximum inhibition exhibited by PECS alone and its composite with MnO_2NPs were obtained at the optimum concentration. Considering the inhibition efficiencies (Z %) of the 4 electrochemical techniques CPP, LPR, EIS and EN, observations indicate there were several variations among the techniques. This is not surprising since there are differences in their experimental configurations such as electrode set up, open circuit voltage periods and other issues such as linearity, causality and stability. Also expected sources of errors such as positions of slope and intercept in determination of Tafel parameters have some parts to play. From Tables 1, 2 and 3, including Figures 5 (a) and (b), PECS exerted elevated inhibition of the metal substrate corrosion in 15 % HCl electrolyte when CPP and EIS techniques are employed followed by LPR and EN in this order.

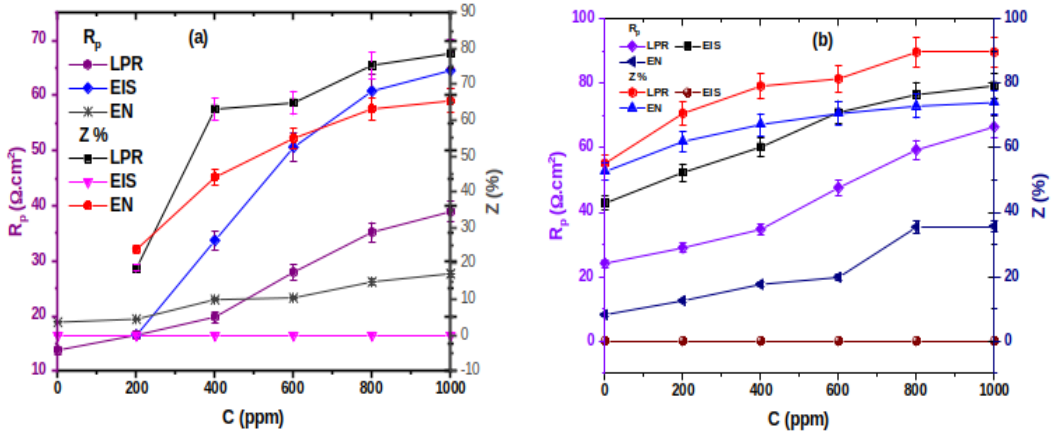

Figure. 10. *Comparison of different electrochemical technique using R_p and Z % obtained from the electrochemical techniques.*

Gouveia-Caridade *et al* [21], postulated that the major difference between EIS and EN can be associated with the configurations used in the setting up of the experiment. For the EIS technique a constant voltage is imposed, which is the same as OCV before the actual commencement of the scan, and variations of local potential on the electrode cross-sections are negligible. However, for EN technique, there is no imposition of external potential, hence the OCV changes more frequently with time particularly during oxide formation. By this method the surface resistance which aligns with that of the oxide film, can be enlarged.

We have explained that CPP and LPR techniques bring out knowledge of events happening at oxidation and reduction branches of the polarization plots. All the parameters for calculating both R_p and Z % in polarization techniques rely on calculation of slope and estimation of intercept points which are variable position determinations. Even though several points are always considered and the average value taken, the source of error still remains. EIS technique gives the most accurate and more quantitative and qualitative information about electrochemical events over a wide range of frequencies and has the most trusted Z % and R_p, devoid of much estimation during calculations.

Figures 10 (a) and (b) show the extent of polarization and metal degradation retardation of the 2 systems of inhibitors at the experimented electrochemical techniques. The 2 sets of systems of inhibition indicate variations of R_p and Z % at the various electrochemical techniques of LPR, EIS and EN. Comparison of the electrochemical techniques with R_p and Z % indicate almost the same pattern of behavior. The scattering and fluctuations in the form of 'zigzag' nature of R_p and Z % plots of the electrochemical techniques have been attributed to the existence of instabilities at the point of introducing the working electrode into the electrolyte and unsteady state characteristics of the electrochemical procedures at the commencement of the experiments [16].

3.7. Thermodynamics Analyses

The adsorption process of inhibitor molecules and ions on substrate cross-sections is an important phenomenon in any corrosion retardation mechanism. This is simply a displacement process where the inhibitor species replace molecules of water which are gradually desorbed from the metal cross-sections [21]. To study the mode of adsorption, values of surface coatings, θ, calculated from retardation efficiencies from the 4 electrochemical techniques were graphically fitted into different empirical and derived adsorption models such as Frumkin, Temkin and Langmuir. The best fit was judged by the given linear plots and the values of R^2 nearness or equal to

unity. Langmuir model which is given by equation (9) [21] gave the nearest approximation:

$$\left(\frac{C_{SM}}{\theta}\right) = \left(\frac{1}{K_{ads}} + C_{SM}\right) \quad (9)$$

where θ is the surface coatings, K_{ads} is the process steady state parameter and C_{SM} is inhibitor concentrations in unit of (ppm).

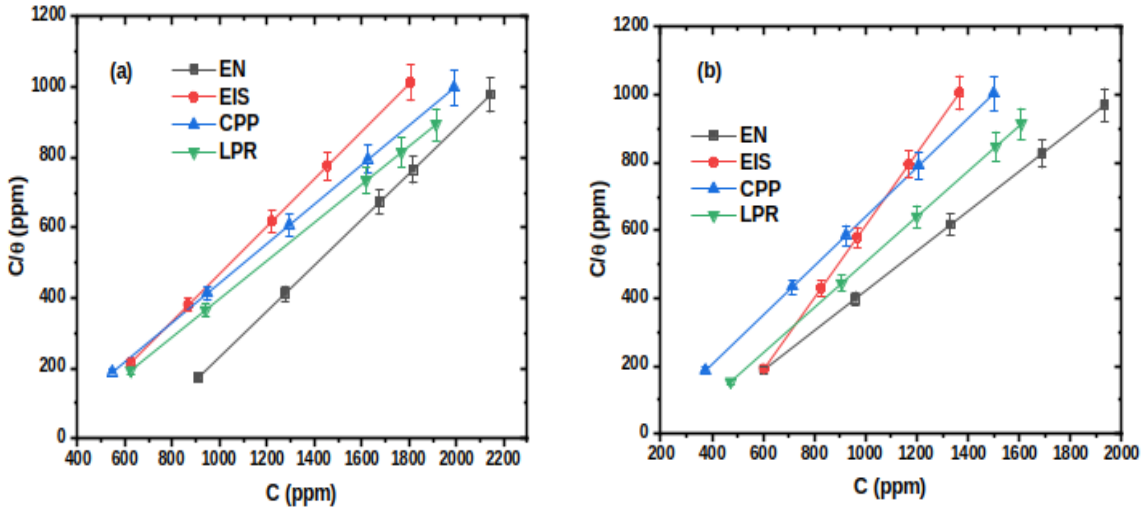

Figure 11. *Langmuir adsorption model for the substrate metal in 15 % HCl solution and inhibited in systems of (a) PECS and (b) PECS+MnO_2NPs.*

Langmuir adsorption model plots were shown as Figures. 11 (a) and (b). In all the techniques, the concentrations progressed as the ratio of concentration to the surface coatings increased. The linear plots obtained can be ascribed to an assumption of an atomic plane accumulation of molecules and ions of inhibitors onto the substrate steel cross-sections. K_{ads} in equation (10) is related to the Gibbs free energy calculated from Langmuir's equation in the following manner:

$$G^{o}_{ads} = -RTln\left(k_{ads} - C_{H_2O}\right) \quad (10)$$

Here C_{H2O} = 55.5 M is water concentration, R = 8.317 kJ/mol is the gas parameter and T is the Kelvin temperature. From Table 4, the ΔG values are all negative, which implies that the adsorption of the biomass extract and the nanoparticles on the cross-sections of the substrate is a spontaneous process [22].

Table 4. *Thermodynamics parameters obtained for system of carbon steel corroding within 15 % HCl and retarded by (a) PECS and (b) PECS+MnO_2NPs.*

System PECS	R^2	K_{ads} (L g^{-1})	ΔG_{ads} (kJmol^{-1})	System PECS+ MnO_2NPs	R^2	K_{ads} (L g^{-1})	ΔG_{ads} (kJmol^{-1})
EN	0.98	0.65 ±0.05	-90.43	EN	0.99	0.59 ±0.02	-29.88
EIS	0.99	0.67 ±0.03	-91.08	EIS	0.99	1.07 ±0.03	-102.88
CPP	0.99	0.56 ±0.01	-86.57	CPP	0.99	0.73 ±0.03	-93.25
LPR	0.92	0.54 ±0.09	-85.65	LPR	0.96	0.67 ±0.08	-91.08

When ΔG_{ads} are < or = 20 kJ/mol, physisorption mode of adsorption prevails which is characterized by electrostatic intermingling between inhibitor molecules and lattice electrons of metal. However, at ΔG_{ads} values = or > 40 kJ/mol, chemisorption mode known for electron transfer and shearing dominates [23]. Therefore, it can be seen that both PECS and

PECS+MnO_2NPs were chemically adsorbed on the substrate, sustained by functional groups present in the biomass extract such as NH_3, -COOH, and so on including the influence of synergistic potency of the nanoparticles.

3.8. Synergism Analyses

Numerous corrosion-based research works had been devoted to investigation about the combined use of 2 or more chemical corrosion retardants to combat metal degradation in aggressive environments. This combined action of 2 or more retardants which are more effective than the individual retardants when used separately is what is known as 'synergism' [8]. Many corrosion scientists have approached the analysis of synergism with the method proposed by Aramaki and Hakerman [21], in which the synergism parameter, S_Q is given by:

$$S_Q = \frac{(1-Q_{1+2})}{(1-Q_{12})} \quad (11)$$

where, $Q_{1+2} = (Q_1 + Q_2) - (Q_2 \times Q_2)$ and Q_1, Q_2, Q_{12} are the values of surface coatings of retardant 1, retardant 2, or combination of the 2 respectively, and are evaluated from experimentally obtained data. The values of S_Q obtained from the 4 electrochemical techniques CPP, LPR, EIS and EN were evaluated and exhibited in Table 5.

Almost all the calculated S_Q are above the threshold of one, used to distinguish whether the combination of two inhibitors, catalysts or drugs manifested synergism, antagonism or additivity. More evidence about synergism can be seen from the various electrochemical techniques where in EIS the introduction of the NPs lead to elevated charge transfer resistances, in CPP reduction in the values of current densities, in LPR increase in polarization resistances and in EN increase in noise resistance.

Table 5. *Synergistic parameter from CPP, LPR, EIS and EN for corrosion retardation of metal substrate in 15 % HCl.*

Sample	Synergism constant (S_Q)			
	CPP	LPR	EIS	EN
200 ppm	1.81	1.16	1.18	0.94
400 ppm	1.77	1.05	1.26	0.83
600 ppm	2.43	1.11	1.09	0.91
800 ppm	2.53	1.01	1.14	1.02
1000 ppm	2.35	1.09	1.32	1.11

3.9. Nanoindentation Analyses and Mechanism of Corrosion Retardation

The load vs depth curves shown in Figure 12 (a), is a measure of nano mechanical characteristics of the substrate metal degrading in belligerent media of 15 % HCl and in the midst of optimum concentrations of chemical corrosion retardants. Nowadays, Corrosion Scientists are employing nano-indentation as a handsome tool to analyse metal degradation products even at micron and nano levels. This has led to broader light into various mechanisms of metal deformations by corrosion and resultant predictions of substrate life span by modeling. The most important information for these are the modulus of elasticity and nano-hardness of the rusts produced from the corrosion process. Thus, Jiang *et al* [24], applied stray current to concrete rods in order to study the corrosion products and obtain numerical data for model predictions. Their investigations yielded modulus of elasticity between 54 and 110 GPa and hardness measured at nano level between 1.8 and 8.3 GPa. These results are in consonant with the values of Young modulus and nano-hardness in Table 6. The steeping feature of unloading part of the nanoindentation curves shown in Figure 12 (a) as load versus depth curves was employed by Oliver and Pharr [25] to estimate modulus of elasticity and nano-hardness. In Figure 12 (a), the steeping goes according to the order of roughness of the carbon steel surface which are in alignment with the work of Jiang *et al* [24].

Figures 12 (b) to (e) exhibit the scanning probe images (SPM) of the carbon steel in the various media while Table 6 shows the corresponding statistical parameters obtained thereof using Gwyddion image analysis software. Considering variables such as surface roughness, root-mean square and peak-to-valley depths in the Table and a survey of the figures indicate that the carbon steel encountered highest protection from degradation in 15 % HCl containing both PECS and MnO_2NPs, followed by PECS and suffered greatest degradation attack in the free acid medium.

Table 6. *Statistical parameters from nano indentation analyses.*

Sample solution	Young modulus (GPa)	Hardness (GPa)	Average surface roughness (Wa) (nm)	Roughness root-average square (Wq) (nm)	Highest peak-to-valley depth (Wp) (nm)
Control (no immersion)	25.52	1.22	96.87	111.18	60.53

Sample solution	Young modulus (GPa)	Hardness (GPa)	Average surface roughness (Wa) (nm)	Roughness root-average square (Wq) (nm)	Highest peak-to-valley depth (Wp) (nm)
Acid free	70.19	4.76	221.32	301.12	202.41
1000 ppm	46.02	3.91	74.04	98.05	31.82
1000 ppm + MnO_2NPs	46.95	3.63	55.92	63.72	21.54

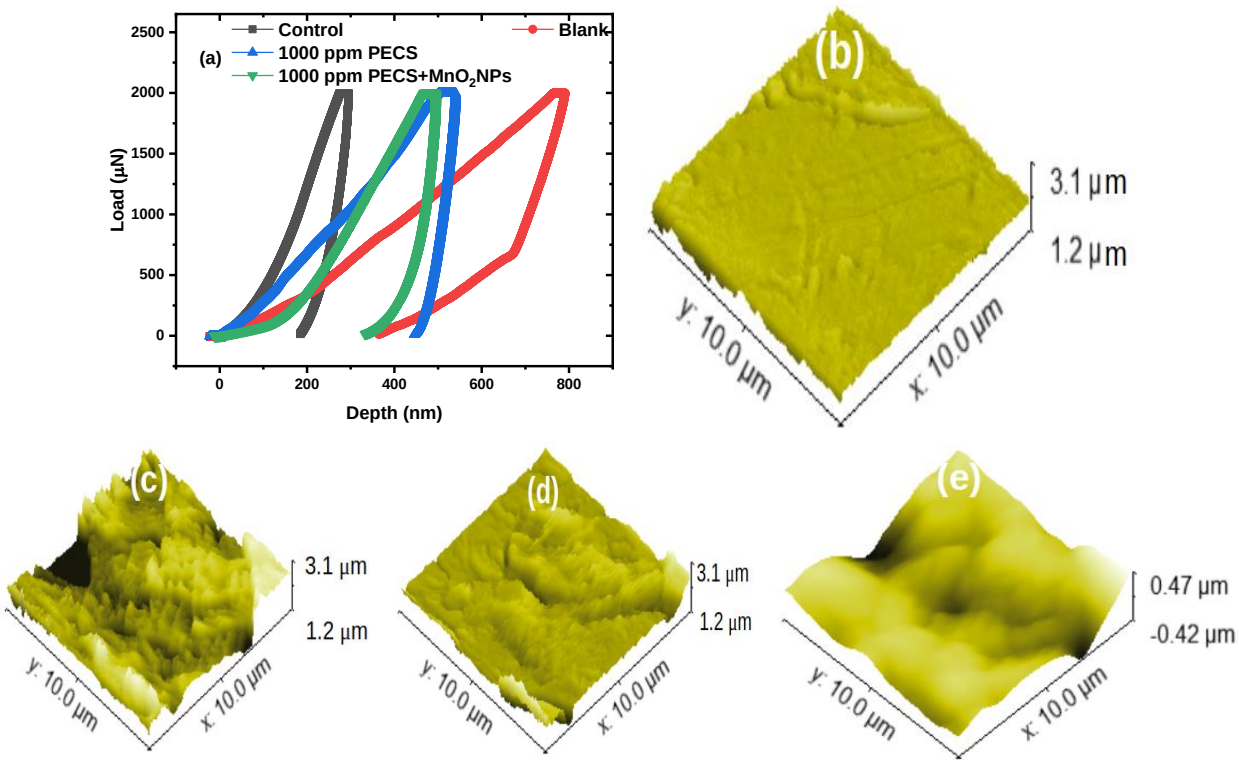

Figure 12. *(a) load vs depth curves, SPM images of (b) control (c) blank (d) 1000 ppm PECS (e) 1000 ppm PECS+MnO_2NPs.*

The synergistic interactions between the pair of PECS and MnO_2NPs can be explained in consideration of a mutual understanding of the nature of molecular mechanisms of corrosion retardation. It seems that PECS and MnO_2NPs mutually support one another in terms of suppression of corrosion and adsorption of inhibitor ions and molecules on metal surfaces. Here the functional groups in the biomass material and molecular size of the nanoparticles play some considerable roles, however, detailed electronic nature and interactions such as formation of bonds, energy release and so on can be solved by molecular dynamics [8, 15].

Evans and Taylor [26] investigated the action of chemical retardants for prevention of deposition of layers of corrosion products on metal cross-sections with cyclic potentiodynamic polarization which involves oxidation and reduction processes. They suggested that a ferrous metal such as carbon steel in an atmospheric environment undergoes dissolution by oxidation to form iron (ii) species such as iron (iii) oxy-hydroxide. However, at the introduction of corrosion retardant species containing heteroatoms such as N, S, O and so on, the heteroatoms interact with the lattice atoms of the metal to form an impervious.

3.10. Comparison of Other Related Works on the Use of Nano-Particles for Corrosion Retardation

Nurislamova *et al.*, [27] suggested that manganese by reason of possession of the same d-orbital in their outermost shell like chromium and close alignment in the periodic table possess almost identical corrosion retardation properties. For example, manganese-containing compounds have a high affinity to oxidize and form complexes, like its counterpart chromium. However, Mn is cheaper because it is obtainable in many ores and its oxides are not poisonous [27]. These issues of economy and environmental friendliness are powerful advantages for future commercialisation of Mn based corro-

sion retardant, Generally, most NPs by the virtue of large volume to surface area disperse easily in belligerent environments to combat agents of metal corrosion [28]. Table 7 presents some parameters from previous works on corrosion inhibition using nano-particles. Here the prospect of chromates replacement with MnO_2NPs can be clearly seen.

Table 7. *Comparison of corrosion retardation performance of different nano-particles.*

S/No	Type of NPs	Basic metal salt	Organic source	Synthesis method	Metal substrate	Electrolyte	Optimum Z %	Reference
1	MnO_2NPs	manganese (ii) acetate	withered rose and lotus petal flowers	ultrasonic wave irradiation	mild steel	1 M HCl	LP (72.63 %) and R_P (51.50 %)	[13]
2	ZnO	$Zn(NO_3)_2$ 6 H_2O	PEG, PVP, and PAN	chemical method	mild steel	5 % HCl	90.81 % (ZnO/PVP)	[7]
3	AgNPs	$AgNO_3$	methacrylic acid	chemical method	aluminium	0.5 M H_2SO_4	85.6 %	[7]
4	AgNPs	$AgNO_3$	honey	sunlight mediation	mild steel	0.5 M HCl	91.6 %	[9]
5	Fe_3O_4NPs	$FeCl_3$	cationic surfactants	chemical method	mild steel	1 M HCl	CPP (89.40), EIS (88)	[26]
6	MnO_2NPs	Potassium permanganate	Orange peels	chemical method	carbon steel	15 % HCl	89.69 %	This present work

4. Conclusion

This research work has so far addressed the sustainable use of carbon steel in a belligerent environment of 15 % HCl and mitigation of its degradation employing a plant extract mediated by Manganese dioxide nanoparticles. The following findings can be used as conclusions:

1. CPP results revealed that the inhibitors manifested mixed inhibition behavior and the retardation efficiencies Z % of PECS+MnO_2NPs are higher than PECS alone, which indicate that the NPs containing composite adsorbs easier on the cross-sections of the carbon steel than PECS alone, leading to elevated Z %.
2. The charge transfer resistance of Nyquist plots of PECS system increased from 4.63 $\Omega.cm^2$ of the free acid solution to 18.38 $\Omega.cm^2$ of optimum concentration while MnO_2NPs system escalated to 37.02 $\Omega.cm^2$. These indicate mass and charge transfer activities leading to continuous formation of more layered coatings on the substrate cross-sections with the improvement of additives concentrations resulting in enhancement of corrosion retardation.
3. Almost all the evaluated synergism constants (S_Q) of each composite mixture of PECS and MnO_2NPs achieved values above the threshold of one which is used to indicate whether synergism or antagonism took place.
4. Comparison of previous research works on the use of NPs for corrosion retardation indicates the prospect of nanoparticles most especially Mn based NPs taking over chromates and its derivatives. Of course this had been done with the patenting of US $6,933,046, a nanoparticles based corrosion retardant which has demonstrated by adhesion, salt fog, and simulated anti-microbial analyses better retardation performance than hexavalent chromium [29].
5. Comparison of the electrochemical techniques with R_p and Z % indicate almost the same pattern of behavior. The scattering and fluctuations in the form of 'zigzag' nature of Rp and Z % plots of the 4 electrochemical techniques have been attributed to the existence of instabilities at the point of introducing the working electrode into the electrolyte and unsteady state characteristics of the electrochemical procedures at the commencement of the experiments [16, 17].
6. This work presents a hopeful prospect for oil and gas industries operators to combat acidizing and other corrosion troublesome operations with nanoparticles based inhibitors, because numerous components of equipment in this sector are made of carbon steel and 15 % HCl is regularly employed in their operations investigated in this research aligns with their industry.

We expect further studies on the use of nanoparticles for corrosion retardation especially Mn based NPs because of its electronic structural relationship with chromium, cheapness and environmental friendliness. Also corrosion tests related to

operating conditions of other industries should be conducted with MnO_2NPs to verify its anti-corrosion efficacy.

Abbreviations

AgNPs	Silver Nanoparticles
CPE	Power Exponent
CPP	Cyclic Potentiodynamic Polarization
C_{SM}	Inhibitor Concentrations
EIS	Electrochemical Impedance Spectroscopy
EN	Electrochemical Noise
E_{corr}	Corrosion Potential
C_{dl}	Double Layer Capacitance
FTIR	Fourier Transform Infrared
ΔG	Gibbs Free Energy
JCPDS	Joint Committee on Powder Diffraction and Standards
K_{ads}	Process Steady State Parameter
LPR	Linear Polarization Resistance
Mn-Ce-P	Manganese - Cerium - Polyphosphate
MnO_2NPs	Manganese Oxide Nanoparticles
PEG	Polyethylene Glycol
PVP	Polyvinylpyrrolidone
PAN	Polyacrilonitrile
R_n	Electrochemical Noise
R_n	Electrochemical Noise Resistance
R_{sol}	Electrolyte Resistance
R_p	Polarization Resistances
SPM	Scanning Probe Microscope
SPR	Surface Plasmon Resonance
XRD	X-Ray Diffractometer
ZRA	Zero Resistance Ammeter

Acknowledgments

We are grateful for contributions from other members of Staff of African Development Bank Laboratory and indeed other academic and non-academic Staff of African University of Science and Technology, Abuja, towards the execution of this research.

Author Contributions

Cyril Onyeka Okoye: Conceptualization, Data curation, Investigation, Project administration, Writing - original draft

Emmanuel Onche: Software, Supervision, Visualization

Abdulhakeem Bello: Data curation, Formal Analysis, Methodology, Validation, Writing - review & editing

Habitat Chaolu: Formal Analysis, Resources, Validation, Visualization, Writing - review & editing

Conflicts of Interest

We solemnly declare that we have no form of competition of interest with anyone or group in this research work.

References

[1] Taylor, C. D.; Gully, B.; S ánchez, A. N.; Rode, E.; Agarwal, A. S. Towards Materials Sustainability through Materials Stewardship. Sustain, 2016, 8 (10), 1-16. https://doi.org/10.3390/su8101001

[2] Northwood, D. O.; Faldu, N. Corrosion: The Circular Materials Economy and Design for Sustainability. In Corrosion and Prevention 2019; 2020; pp 1-16.

[3] Umoren, S. A.; Solomon, M. M.; Obot, I. B.; Suleiman, R. K. A Critical Review on the Recent Studies on Plant Biomaterials as Corrosion Inhibitors for Industrial Metals. J. Ind. Eng. Chem., 2019, 76, 91-115.

[4] Dhand, V.; Soumya, L.; Bharadwaj, S.; Chakra, S.; Bhatt, D.; Sreedhar, B. Green Synthesis of Silver Nanoparticles Using Coffea Arabica Seed Extract and Its Antibacterial Activity. Mater. Sci. Eng. C, 2016, 58, 36-43.

[5] Jain, P.; Patidar, B.; Bhawsar, J. Potential of Nanoparticles as a Corrosion Inhibitor: A Review. J Bio Tribo Corros, 2020, 6 (43).

[6] Solomon, M. M.; Gerengi, H.; Umoren, S. A. Carboxymethyl Cellulose/Silver Nanoparticles Composite: Synthesis, Characterization and Application as a Benign Corrosion Inhibitor for St37 Steel in 15% H2SO4 Medium. ACS Appl. Mater. Interfaces, 2017, 9 (7), 6376-6389. https://doi.org/10.1021/acsami.6b14153

[7] Quadri, T. W.; Olasunkanmi, L. O.; Fayemi, O. E.; Solomon, M. M.; Ebenso, E. E. Zinc Oxide Nanocomposites of Selected Polymers : Synthesis, Characterization, and Corrosion Inhibition Studies on Mild Steel in HCl Solution. ACS Omega, 2017, 2, 8421-8437. https://doi.org/10.1021/acsomega.7b01385

[8] Solomon, M. M.; Umoren, S. A. Performance Assessment of Poly(Methacrylic Acid)/Silver Nanoparticles Composite as Corrosion Inhibitor for Aluminium in Acidic Environment. J. Adhes. Sci. Technol., 2015, 29(21), 2311-2333.

[9] Obot, I. B.; Umoren, S. A.; Johnson, A. S. Sunlight- Mediated Synthesis of Silver Nanoparticles Using Honey and Its Promising Anticorrosion Potentials for Mild Steel in Acidic Environments. J. Mater. Environ. Sci., 2013, 4 (6), 1013-1018.

[10] Azzam, E. M. S.; Abd El-Aal, A. A. Corrosion Inhibition Efficiency of Synthesized Poly 12-(3-Amino Phenoxy) Dodecane-1-Thiol Surfactant Assembled on Silver Nanoparticles. Egypt. J. Pet., 2013, 22 (2), 293-303. https://doi.org/10.1016/j.ejpe.2013.06.008

[11] Safety Data Sheet, "Manganese Nanoparticles".

[12] Jian, S. Y.; Tzeng, Y. C.; Ger, M. Der; Chang, K. L.; Shi, G. N.; Huang, W. H.; Chen, C. Y.; Wu, C. C. The Study of Corrosion Behavior of Manganese-Based Conversion Coating on LZ91 Magnesium Alloy: Effect of Addition of Pyrophosphate and Cerium. Mater. Des., 2020, 192, 108707. https://doi.org/10.1016/j.matdes.2020.108707

[13] Syed Khadar, Y. A.; Surendhiran, S.; Gowthambabu, V.; Halimabi Alias Shakila Banu, S.; Devabharathi, V.; Balamurugan, A. Enhancement of Corrosion Inhibition of Mild Steel in Acidic Media by Green-Synthesized Nano-Manganese Oxide. Mater. Today Proc., 2021, 47 (May), 889-893. https://doi.org/10.1016/j.matpr.2021.04.335

[14] Abd-El-nabey, B. A.; Abd-El-khalek, D. E.; El-Housseiny, S.; Mohamed, M. E. Plant Extracts as Corrosion and Scale Inhibitors: A Review; 2020; Vol. 9. https://doi.org/10.17675/2305-6894-2020-9-4-7

[15] Obot, I. B.; Kumar, A. M.; Umoren, S. A.; Gasem, Z. Surface Protection of Mild Steel Using Benzimidazole Derivatives: Experimental and Theoretical Approach. J. Adhes. Sci. Technol., 2015, 29(19), 2130-2152. https://doi.org/https://doi.org/10.1080/01694243.2015.1058544

[16] Meeusen, M.; Zardet, L.; Homborg, A. M.; Lekka, M.; Andreatta, F.; Fedrizzi, L.; Boelen, B.; Terryn, H.; Mol, J. M. C. A Complementary Electrochemical Approach for Time-Resolved Evaluation of Corrosion Inhibitor Performance. J. Electrochem. Soc., 2019, 166 (11), C3220-C3232. https://doi.org/10.1149/2.0271911jes

[17] Hussin, M. H.; Rahim, A. A.; Mohamad Nasir Mohamad Ibrahim; Brosse, N. The Capability of Ultrafiltrated Alkaline and Organosolv Oil Palm (Elaeis Guineensis) Fronds Lignin as Green Corrosion Inhibitor for Mild Steel in 0.5 M HCl Solution. Measurement, 2016, 28, 90-103.

[18] Loveday, D. Electrochemical Corrosion Rate Measurement - A Comparison.

[19] Lazanas, A. C.; Prodromidis, M. I. Electrochemical Impedance Spectroscopy─A Tutorial. ACS Meas. Sci. Au, 2023, 3 (3), 162-193. https://doi.org/10.1021/acsmeasuresciau.2c00070

[20] Montoya-Rangel, M.; de Oca, N. G. M.; Gaona-Tiburcio, C.; Colás, R.; Cabral-Miramontes, J.; Nieves-Mendoza, D.; Maldonado-Bandala, E.; Chacón-Nava, J.; Almeraya-Calderón, F. Electrochemical Noise Measurements of Advanced High-Strength Steels in Different Solutions. Metals (Basel), 2020, 10 (9), 1-20. https://doi.org/10.3390/met10091232

[21] Gouveia-Caridade, C.; Pereira, M. I. S.; Brett, C. M. A. Electrochemical Noise and Impedance Study of Aluminium in Weakly Acid Chloride Solution. Electrochim. Acta, 2004, 49 (5), 785-793.

[22] Abbass, M. K.; Raheef, K. M.; Aziz, I. A.; Hanoon, M. M.; Mustafa, A. M.; Al-Azzawi, W. K.; Al-Amiery, A. A.; Kadhum, A. A. H. Evaluation of 2-Dimethylaminopropionamidoantipyrine as a Corrosion Inhibitor for Mild Steel in HCl Solution: A Combined Experimental and Theoretical Study. Prog. Color. Color. Coatings, 2024, 17 (1), 1-10. https://doi.org/10.30509/pccc.2023.167081.1197

[23] Okoye, C. O.; Odette, F.; Bello, A.; Itodo, J. E.; Onche, E. O.; Okon, E. N. Metronidazole Mediated Potassium Iodide as High-Performance Deterioration Retardant for Mild Steel in an Acidic Media. J. Dispers. Sci. Technol., 2024, 1-12. https://doi.org/10.1080/01932691.2024.2348493

[24] Jiang, B.; Doi, K.; Tsuchiya, K.; Kawano, Y.; Kori, A.; Ikushima, K. Micromechanical Properties of Steel Corrosion Products in Concrete Studied by Nano-Indentation Technique. Corros. Sci., 2019, 163, 1-31. https://doi.org/10.1016/j.corsci.2019.108304

[25] Oliver, W. C.; Pharr, G. M.; Introduction, I. An Improved Technique for Determining Hardness and Elastic Modulus Using Load and Displacement Sensing Indentation Experiments. Mater. Res., 1992, 7 (6).

[26] Bijapur, K.; Molahalli, V.; Shetty, A.; Toghan, A.; De Padova, P.; Hegde, G. Recent Trends and Progress in Corrosion Inhibitors and Electrochemical Evaluation. Appl. Sci., 2023, 13 (18). https://doi.org/10.3390/app131810107

[27] Nurislamova, E. A.; Ziganshina, M. R.; Stepin, S. N.; Mendelson, V. A. Anticorrosion Properties of Manganese-Containing Complex Oxides, Obtained by Stoneware Method. IOP Conf. Ser. Mater. Sci. Eng., 2020, 905 (1), 1-7. https://doi.org/10.1088/1757-899X/905/1/012051

[28] Chandrasekaran, S.; Surendhiran, S.; Benham, A.; Sudha, M.; Gopinath, B.; Khadar, Y. A. S.; Balamurugan, A. Enhancement of Marine Corrosion Inhibition of Mild Steel by Fabrication of Environmental Friendly CeO2 Coating. in INTERNATIONAL CONFERENCE ON ADVANCES IN MATERIALS, COMPUTING AND COMMUNICATION TECHNOLOGIES: (ICAMCCT 2021); 2022.

[29] Elliott, J. Nanoparticle-Based Corrosion Inhibitors for Aerospace Aluminum. In Tri-Service Corrosion Conference; 2007; pp 1-7.